



ALMA MATER STUDIORUM  
UNIVERSITÀ DI BOLOGNA

ARCHIVIO ISTITUZIONALE  
DELLA RICERCA

Alma Mater Studiorum Università di Bologna  
Archivio istituzionale della ricerca

Experimental validation of a two equation RANS transitional turbulence model for compressible microflows

This is the final peer-reviewed author's accepted manuscript (postprint) of the following publication:

*Published Version:*

Experimental validation of a two equation RANS transitional turbulence model for compressible microflows / Rehman D.; Morini G.L.. - In: INTERNATIONAL JOURNAL OF HEAT AND FLUID FLOW. - ISSN 0142-727X. - ELETTRONICO. - 86:(2020), pp. 108711.1-108711.11. [10.1016/j.ijheatfluidflow.2020.108711]

*Availability:*

This version is available at: <https://hdl.handle.net/11585/776679> since: 2020-10-29

*Published:*

DOI: <http://doi.org/10.1016/j.ijheatfluidflow.2020.108711>

*Terms of use:*

Some rights reserved. The terms and conditions for the reuse of this version of the manuscript are specified in the publishing policy. For all terms of use and more information see the publisher's website.

This item was downloaded from IRIS Università di Bologna (<https://cris.unibo.it/>).  
When citing, please refer to the published version.

(Article begins on next page)

This is the final peer-reviewed accepted manuscript of:

Danish Rehman, Gian Luca Morini,

**Experimental validation of a two equation RANS transitional turbulence model for compressible microflows**

International Journal of Heat and Fluid Flow, Volume 86, 2020, 108711

The final published version is available online at:

<https://doi.org/10.1016/j.ijheatfluidflow.2020.108711>

Rights / License:

The terms and conditions for the reuse of this version of the manuscript are specified in the publishing policy. For all terms of use and more information see the publisher's website.

*This item was downloaded from IRIS Università di Bologna (<https://cris.unibo.it/>)*

***When citing, please refer to the published version.***

# Experimental Validation of a Two Equation RANS Transitional Turbulence Model for Compressible Microflows

Danish Rehman<sup>a</sup>, Gian Luca Morini<sup>a</sup>

<sup>a</sup> *Microfluidics Laboratory, Dept. of Industrial Eng. Via del Lazzaretto 15/5, University of Bologna, Bologna 41031, Italy*

---

## Abstract

Laminar-to-turbulent flow transition in microchannels can be useful to enhance mixing and heat transfer in microsystems. Typically, the small characteristic dimensions of these devices hinder in attaining higher Reynolds numbers to limit the total pressure drop. This is true especially in the presence of a liquid as a working medium. On the contrary, due to lower density, Reynolds number larger than 2000 can be easily reached for gas microflows with an acceptable pressure drop. Since microchannels are used as elementary building blocks of micro heat exchangers and micro heat-sinks, it is essential to predict under which conditions, the laminar-to-turbulent flow transition inside such geometries can be expected. In this paper, experimental validation of a two equations transitional turbulence model, capable of predicting the laminar-to-turbulent flow transition for internal flows as proposed by [Abraham et al. \(2008\)](#), is presented for the first time for microchannels. This is done by employing microchannels in which Nitrogen gas is used as a working fluid. Two different cross-sections namely circular and rectangular are utilized for numerical and experimental investigations. The inlet mass flow rate of the gas is varied to cover all the flow regimes from laminar to fully turbulent flow. Pressure loss experiments are performed for both cross-sectional geometries and friction factor results from experiments and numerical simulations are compared. From the analysis of the friction factor as a function of the Reynolds number, the critical value of the Reynolds number linked to the laminar-to-turbulent transition has been deter-

mined. The experimental and numerical critical Reynolds number for all the tested microchannels showed a maximum deviation of less than 12%. These results demonstrate that the transitional turbulence model proposed by Abraham et al. (2008) for internal flows can be extended to microchannels and proficiently employed for the design of micro heat exchangers in presence of gas flows.

*Keywords:* compressibility, laminar-to-turbulent flow transition, friction factor, micro heat exchangers

---

## 1. Introduction

The prediction of the laminar-to-turbulent transition in microtubes (MTs) and microchannels (MCs) is very important for the design of microdevices in which internal flows are present such as heat sinks and micro heat exchangers. After the pioneering work of Tuckerman and Pease (1981), most of the earlier experimental groups involved in the analysis of internal flows within microchannels reported an anticipated laminar-to-turbulent flow transition in MCs like Peiyi and Little (1983), Choi et al. (1991), Peng et al. (1994) among others. Whereas, a few groups like Harms et al. (1999), Adams et al. (1999) confirmed the agreement to the typical rules of the laminar-to-turbulent transition in conventional tubes. Recent reviews like those of Asadi et al. (2014), Dixit and Ghosh (2015) conclude that experimental data obtained in the recent decade seems to confirm that single-phase flows in MCs follow conventional laws. A comprehensive review outlining possible reasons for deviations from macro theory in earlier reported experiments is due to Morini (2004b), according to which macro theory holds for MC flows as long as scaling effects can be considered negligible. Morini (2004b) individuated the main scaling effects (compressibility, rarefaction, viscous dissipation, electro osmotic effects, and surface roughness) that need to be verified before interpreting experimental results which can be responsible for deviation from conventional correlations. In another work, Morini (2004a) gathered previously published experimental data for laminar-to-turbulent flow transition in MCs and compared them with macro laws. The analysis in rectan-

gular microchannels showed that various published results for critical Reynolds number ( $Re_c$ ) can be explained by using the Obot-Jones model developed for  
25 conventional channels with a cross-section different from circular (which is the case of large part of microchannels). In fact, [Obot \(1988\)](#) demonstrated that the critical Reynolds number linked to the laminar-to-turbulent transition is a function of the cross-sectional geometry of the channel.

Laminar-to-turbulent flow transition even in conventional sized channels is  
30 still an open field of investigation. Based on original experiments of [Reynolds \(1883\)](#), the transition in pipe flow occurs when the Reynolds number reaches a critical value ( $Re_c$ ) close to 2000 in the presence of a tube with a rough entrance. The full comprehension of the physical processes, which trigger such flow transition when the flow rate is increased, is yet to be achieved. Thus, research  
35 investigation in this domain is very active using sophisticated experimental and theoretical approaches, as evidenced by the works of [Barkley et al. \(2010\)](#), [Avila et al. \(2011\)](#), [Barkley et al. \(2011\)](#). Pipe flow experiments of [Avila et al. \(2011\)](#) showed that when the flow velocity is such that  $Re$  is lower than its critical value, turbulence was not sustained. Even if turbulent puffs were generated in  
40 the flow field, they were decayed swiftly by the surrounding laminar flow when the  $Re$  was lower than its critical value. This process is referred to as relaminarization. Above  $Re_c = 2040$ , the splitting process of these turbulent puffs outweighed the decay and hence turbulence could sustain. Afterward, turbulent puffs increased their size and the whole flow field suddenly exhibited a disor-  
45 dered motion. Later, [Barkley et al. \(2011\)](#) performed experiments on 10 *mm* pipe and 5 *mm* square duct. They introduced the perturbations in the flow field at a precise location along the length to initiate the turbulence. They also conducted Direct Numerical Simulations (DNS) of the flow field and showed that even when the flow is fully turbulent, just by modifying the velocity profile to  
50 more plug shaped caused the fully turbulent flow to break into turbulent puffs that were experimentally observed for  $Re < 2300$ . Such DNS inspired experiments were then conducted by [Kühnen et al. \(2018\)](#) who demonstrated how sustained turbulence can be destabilized and flow relaminarized in the pipe. Si-

milarly, flow visualization as well as pressure drop studies, have been utilized to  
55 determine  $Re_c$  for microflows (Li and Olsen (2006), Wibel and Ehrhard (2009),  
Kim (2016)).

Due to the large difference in terms of density between working fluid and  
seeding particles, optical experimental techniques like  $\mu$ PIV are not recommen-  
ded for gas flows in MCs and therefore a pressure drop study (Moody chart)  
60 remains the only useful experimental tool to determine the critical value of the  
Reynolds number ( $Re_c$ ). Such analysis for gas flows in 11 different microtubes  
with  $D_h = 125 - 180 \mu m$  has been presented by Morini et al. (2009). By compar-  
ing their results with previously published gas flow pressure drop studies, it  
was shown that if friction factor is calculated by taking into account compress-  
65 sibility effects and minor losses,  $Re_c$  was in between 1800 – 2000, in complete  
disagreement with the earlier transitions reported by other groups like Peiyi and  
Little (1983), Kandlikar et al. (2005).

As highlighted earlier, aside from experimental and analytical observations,  
DNS has been applied to understand the physics of flow transition like in the case  
70 of Barkley et al. (2011), Wu et al. (2015), Kühnen et al. (2018). However, due  
to the lower computational cost, Reynolds-Averaged Navier Stokes equations  
(RANS) based turbulence modeling is still preferred in industrial environments  
for engineering design goals. A breakthrough in modeling transitional flow using  
two equations turbulence models is due to Menter et al. (2006). They augmen-  
75 ted the original Shear Stress Transport (SST)  $k - \omega$  model (Menter (1994)) to  
incorporate flow transition based upon two additional intermittency transport  
equations. This model was later modified to be implemented into commercial  
CFD codes (Menter and Langtry (2012)). Although originally developed for  
external flows, constants present in the Menter’s model were modified by Abra-  
80 ham et al. (2008) to predict laminar-to-turbulent transition in internal flows. It  
was shown for pipe flow that the fine-tuned model predicted laminar and fully  
turbulent friction factors similar to that of Poiseuille’s law and Blasius law re-  
spectively. Therefore, transitional behavior was deemed to be representative of  
reality. The modification proposed by Abraham et al. (2008) for the transitional

85 turbulence model of [Menter et al. \(2006\)](#) has not been validated experimentally for internal flows nor for microchannels. Considering this, the current work aims to experimentally validate this transitional turbulence model for gas microflows using the modified form as proposed by [Abraham et al. \(2008\)](#). The experimental validation will be made by observing the variation of the values assumed by  
 90 the friction factor as a function of the Reynolds number. Both semi-local and average values of friction factors will be used in this validation.

## 2. Experimental Setup and Data Reduction

Pressure loss experiments are performed for a commercial MT (Upchurch<sup>®</sup>) and two rectangular MCs fabricated by milling a PMMA plastic sheet using  
 95 a micromilling machine (Roland<sup>®</sup> MDX-40A). Dimensions and inner surface roughness of MCs are measured using an optical profiler (Talysurf CCI). For MT, a value of the surface roughness similar to that of [Morini \(2004a\)](#), [Morini et al. \(2009\)](#), [Yang \(2012\)](#), was extracted from SEM imaging of the stainless steel MTs. The measured average width ( $w$ ), height ( $h$ ), aspect ratio ( $\alpha =$   
 100  $h/w$ ) and surface roughness ( $\varepsilon$ ) of investigated channels are reported in Table [1](#). Experimental test bench and a schematic of MC assembly used in this work are

Table 1: Channels geometry used for experiments.

Channel	$h$ ( $\mu\text{m}$ )	$w$ ( $\mu\text{m}$ )	$\alpha$	$D_h$ ( $\mu\text{m}$ )	$\varepsilon$ ( $\mu\text{m}$ )
MT	-	-	1	1016	1
MC1	250	360	0.694	295	1.05
MC2	134	554	0.241	215	0.9

shown in Figure [1](#). Pressurized Nitrogen gas is allowed to enter MC assembly perpendicular to the axial direction of MC and leaves perpendicularly as well through the outlet manifold. In the case where experiments are performed for  
 105 circular cross section, MC assembly is simply replaced by attaching MT directly at the inlet of the test bench using a commercial reducer/manifold. The total pressure drop between the inlet and the outlet of the MC/MT assembly is

measured by means of a differential pressure transducer (Validyne DP15) with an interchangeable sensing element that allows accurate measurements over the whole range of encountered pressures. Atmospheric pressure is measured using an absolute pressure sensor (Validyne AP42). To measure the temperature at the entrance of the MC/MT assembly a K-type, calibrated thermocouple is used. Thermocouple voltage and an amplified voltage of pressure sensors are fed to internal multiplexer board of Agilent 39470A which is used as a switch. Voltages from the switch are measured using Agilent 34420A with a 7 – 1/2 digits resolution and are finally stored in a PC using a Labview<sup>®</sup> program.

Considering one dimensional flow of ideal gas, average Fanning friction factor between inlet 'in' and outlet 'out' of a MC/MT with length  $L$  can be obtained by using the following expression for a compressible flow as indicated by [Kawashima and Asako \(2014\)](#):

$$f_f = \frac{D_h}{L} \left[ \frac{p_{in}^2 - p_{out}^2}{RT_{av}\dot{G}^2} - 2 \ln \left( \frac{p_{in}}{p_{out}} \right) + 2 \ln \left( \frac{T_{in}}{T_{out}} \right) \right] \quad (1)$$

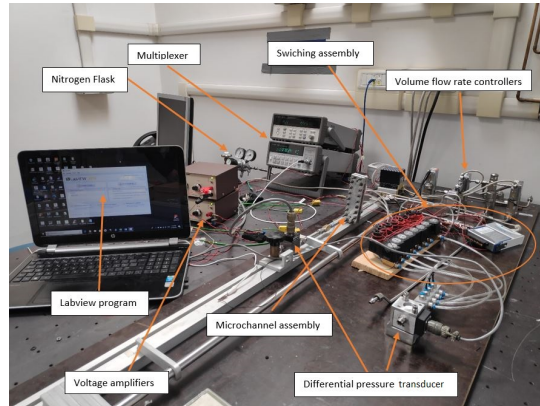
where  $p$  and  $T$  denote cross sectional average pressure and temperature of the gas and the subscripts 'in' and 'out' represent the inlet and the outlet of MC/MT, respectively.  $T_{av}$  is the average temperature of the gas between inlet and outlet of MC/MT, and  $\dot{G}$  is the mass flux ( $\dot{G} = \frac{\dot{m}}{A}$ ). Hydraulic diameter of a rectangular MC is defined as:

$$D_h = \frac{2wh}{w + h} \quad (2)$$

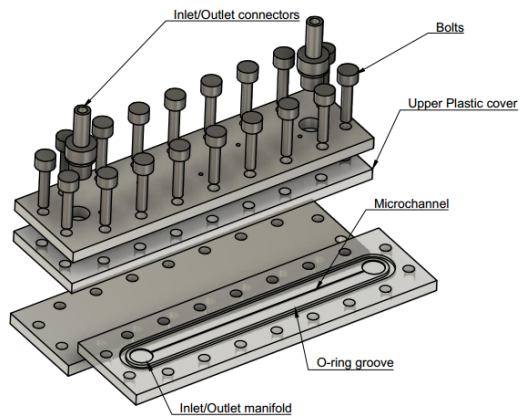
Reynolds number at the inlet of MC/MT can then be calculated using measured mass flow rate and calculated viscosity at inlet temperature with the following equation:

$$Re = \frac{\dot{m}D_h}{\mu A} \quad (3)$$

In addition, under the hypothesis of adiabatic compressible flow, the energy balance for one dimensional Fanno flow, between inlet 'in' and any other cross section at a distance 'x' from the inlet of the MC/MT yields the following quadratic equation for the estimation of average cross-sectional temperature as



(a)



(b)

Figure 1: Experimental setup (a), and an exploded view of MC assembly (b).

demonstrated by [Kawashima and Asako \(2014\)](#):

$$\left(\frac{\rho_{in}^2 u_{in}^2 R^2}{2c_p p_x^2}\right) T_x^2 + T_x - \left(T_{in} + \frac{u_{in}^2}{2c_p}\right) = 0 \quad (4)$$

Finally, knowing the average pressure and temperature **in a specific cross-section**,  
 135 average density and velocity of compressible gas can be obtained using the ideal  
 gas law (Eq. [8](#)) and continuity equations, respectively. An initial estimate of  
 the gas velocity at MC/MT inlet is made using the measured mass flow rate  
 and density of the gas at the inlet manifold entrance. MC/MT inlet properties  
 are then calculated by assuming an isentropic expansion between the inlet of  
 140 the assembly and the MC/MT. For further **details on the equations** that are  
 solved iteratively to determine the inlet flow properties, the reader is referred to  
 the previous works ([Rehman et al. \(2019\)](#), [Hong et al. \(2016\)](#)). Once inlet con-  
 ditions are determined, temperature at MC/MT outlet can be easily evaluated  
 using Eq. [4](#) given the local pressure is known. In current work, a hypothesis of  
 145 perfect expansion is considered which essentially assumes atmospheric pressure  
 at the MC/MT outlet ( $p_{out} = p_{atm}$ ). This assumption holds if the dynamic  
 conditions of gas flow are far from choking ([Rehman et al. \(2019\)](#)). Utilizing  
 the outlet temperature evaluated by Eq. [4](#) and under perfect expansion assump-  
 tion, average Fanning friction factor of MC/MT can finally be calculated using  
 150 Eq. [1](#).

In order to assess the accuracy of the experimental measurements, the un-  
 certainty associated to each instrument used in the experimental campaigns is  
 reported in Table [2](#). In a detailed study, [Yang \(2012\)](#), based on the theory of

Table 2: Typical uncertainties of instruments used.

Instrument	Range (0–Full Scale (FS))	Uncertainty
Volume flow rate controllers	0–5000 mL/min	± 0.5% FS
Pressure sensors	0–22, 0–86 & 0–1460 kPa	± 0.25% FS
K-type thermocouple	0–100 °C	± 0.25% FS

error propagation, highlighted that uncertainty in the evaluation friction factor

155 is highly influenced by the uncertainty on the hydraulic diameter. In the present case, the uncertainty on the hydraulic diameter, evaluated by using an optical profilometer to measure both height ( $h$ ) and width ( $w$ ) of the MC, is of the order of 1.5%. The uncertainty associated to the measurement of  $L$  is around 0.4%. Therefore, the uncertainty in evaluating  $f_f$  (with Eq. [1](#)) and  $Re$  (with Eq. [3](#)) is  
160 estimated to be equal to  $\pm 10\%$  and  $\pm 3\%$ , respectively. All these uncertainties are summarized in Table [3](#).

Table 3: Typical uncertainties of experimentally deduced parameters based on theory of propagation.

Calculated Parameter	Uncertainty
$D_h$	$\pm 5\%$
$Re$	$\pm 3\%$
$f_f$	$\pm 10\%$

### 3. Mathematical Model

Internal flow physics of a compressible gas is governed by the following conservation equations of mass, momentum and energy:

$$\frac{\partial \rho u_i}{\partial x_i} = 0, \quad (5)$$

165

$$\frac{\partial \rho u_i}{\partial t} + \frac{\partial}{\partial x_j} \rho(u_j u_i) = -\frac{\partial p}{\partial x_i} + (\mu + \mu_t) \frac{\partial^2 u_i}{\partial x_j \partial x_j}, \quad (6)$$

$$\rho C_\mu u_i \frac{\partial T}{\partial x_i} = -p \frac{\partial u_i}{\partial x_i} + \lambda \frac{\partial^2 T}{\partial x_i^2} - \tau_{ij} \frac{\partial u_j}{\partial x_i}, \quad (7)$$

where  $i, j=1,2,3$  are used to indicate three spatial directions;  $u_i$  represents the Cartesian velocity components in longitudinal, lateral and normal directions respectively;  $p$  is the pressure;  $\rho$  is the fluid density;  $T$  is the average fluid cross  
170 sectional temperature,  $\mu$  is the fluid dynamic viscosity and  $\mu_t$  is turbulent viscosity. For a laminar compressible fluid flow, there are 6 unknowns ( $u, v, w, p, \rho, T$ ) for aforementioned set of 5 equations from Eqs. [\(5\)](#)-[\(7\)](#). An additional constitutive law is therefore used to complete the solution procedure for the complete

set of Navier Stokes (NS) equations, as follows:

175

$$p = \rho RT, \quad (8)$$

where  $R$  is the specific gas constant. In order to proceed for a steady state solution of turbulent Reynold average NS (RANS) equations, the closure problem has been addressed in the literature by various models such as  $k - \epsilon$  (Launder and Spalding (1974)) and Wilcox  $k - \omega$  (Wilcox (1988, 2008)), to name a few.

180

In the current work a shear stress transport (SST) model presented by Menter (1994) is used. This model uses  $k - \omega$  approximation close to the walls and switches to  $k - \epsilon$  far from the wall. The closure problem is dealt with the following two transport equations for modelling turbulent kinetic energy ( $k$ ) and specific rate of turbulent destruction ( $\omega$ ):

185

$$\frac{\partial(\rho u_i k)}{\partial x_i} = P_k - \beta_1 \rho k \omega + \frac{\partial \left( \left( \mu + \frac{\mu_t}{\sigma_k} \right) \frac{\partial k}{\partial x_i} \right)}{\partial x_i}, \quad (9)$$

$$\frac{\partial(\rho u_i \omega)}{\partial x_i} = \chi \rho S^2 - \beta_2 \rho k \omega^2 + \frac{\partial \left( \left( \mu + \frac{\mu_t}{\sigma_\omega} \right) \frac{\partial \omega}{\partial x_i} \right)}{\partial x_i} + 2(1 - F_1) \rho \frac{1}{\sigma_{\omega 2} \omega} \frac{\partial k}{\partial x_i} \frac{\partial \omega}{\partial x_i}, \quad (10)$$

where  $P_k$  is the rate of kinetic energy production,  $\sigma_k$  and  $\sigma_\omega$  are the equivalents of Prandtl number for the transport of turbulent kinetic energy and specific rate of turbulent destruction, respectively. Moreover subscripts 1 and 2 for these  $\sigma_k$  and  $\sigma_\omega$  represent different constants assumed for original  $k - \omega$  model close to the wall and  $k - \epsilon$  far from the wall, respectively.  $S$  is the absolute value of shear strain rate and  $\chi$ ,  $\beta_1$  &  $\beta_2$  are SST model constants.  $F_1$  is a blending function that allows to switch from standard  $k - \epsilon$  model to  $k - \omega$  in order to better simulate the low Reynolds number region.

190

195

For most industrial problems, laminar flows are solved by NS equations whereas turbulent flows are dealt with RANS equations as described above. In the transitional flow regime between laminar and turbulent, computationally expensive models such as Large Eddy Simulations (LES) and DNS are applied where the transient evolution of the turbulence scales is modelled in the computational

200 domain. Although accurate in predictions of flow characteristics, computational cost associated to these modelling techniques is enormous as compared to RANS and therefore are limited to accurate scientific evaluations. The two equation transport model (RANS) due to [Menter et al. \(2006\)](#) is coupled to two additional transport equations for the evaluation of a so called intermittency  
 205 factor ( $\gamma$ ). Its role is to diminish turbulence production for flow conditions that are not fully turbulent and its value is between 0 and 1. Evaluation of  $\gamma$  however, depends on another local flow property, the momentum thickness Reynolds ( $\tilde{Re}_{\theta t}$ ), which describes the local stability status of the flow in the near wall region. These two additional transport equations are the following:

$$210 \quad \frac{\partial(\rho\gamma)}{\partial t} + \frac{\partial(\rho u_i \gamma)}{\partial x_i} = P_{\gamma 1} - E_{\gamma 1} + P_{\gamma 2} - E_{\gamma 2} + \frac{\partial \left( \left( \mu + \frac{\mu_t}{\sigma_f} \right) \frac{\partial \gamma}{\partial x_i} \right)}{\partial x_i} \quad (11)$$

$$\frac{\partial(\rho \tilde{Re}_{\theta t})}{\partial t} + \frac{\partial(\rho u_i \tilde{Re}_{\theta t})}{\partial x_i} = P_{\theta t} + \frac{\partial \left( \sigma_{\theta t} (\mu + \mu_t) \frac{\partial \tilde{Re}_{\theta t}}{\partial x_i} \right)}{\partial x_i} \quad (12)$$

A detailed explanation of all the terms of Eqs. [\(11\)](#) and [\(12\)](#) can be found in [Menter et al. \(2006\)](#), [ANSYS \(2018\)](#). Only the most relevant terms are presented here starting from the transition source in Eq. [\(11\)](#) for intermittency:

$$215 \quad P_{\gamma 1} = F_{length} \rho S (\gamma F_{onset})^{c_{a1}} \quad (13)$$

$$E_{\gamma 1} = c_{e1} P_{\gamma 1} \gamma \quad (14)$$

where  $F_{onset}$  is used to trigger the intermittency  $\gamma$  production and its formulation is a function of vorticity Reynolds number  $Re_\nu = \frac{\rho y^2 S}{\mu}$  [ANSYS \(2018\)](#).  $F_{length}$  is obtained from correlations and it is dependent on  $\tilde{Re}_{\theta t}$ ; the detail  
 220 about the correlations proposed for these two terms can be found in [Menter and Langtry \(2012\)](#). In Eq. [\(11\)](#), the destruction/relaminarization sources are defined as follows:

$$P_{\gamma 2} = c_{a2} \rho \Omega \gamma F_{turb} \quad (15)$$

$$E_{\gamma 2} = c_{e2} P_{\gamma 2} \gamma \quad (16)$$

where  $\Omega$  denotes the magnitude of the absolute vorticity rate,  $F_{turb} = e^{-\left(\frac{R_t}{4}\right)^4}$  and  $R_t = \frac{\rho k}{\mu \omega}$ . Another important term in Eq. [\(11\)](#) is the production of  $\tilde{Re}_{\theta t}$ ,

225 defined as follows:

$$P_{\theta t} = c_{\theta t} \frac{\rho}{t} (Re_{\theta t} - \tilde{R}e_{\theta t})(1 - F_{\theta t}) \quad (17)$$

where  $t$  is a time scale that is present for dimensional reason and  $F_{\theta t}$  is a blending function that allows to turn off the source terms in the boundary layer where the scalar quantity  $\tilde{R}e_{\theta t}$  is only diffusing.

Coupling between the intermittency equations and SST model can be done by multiplying  $\gamma$  to the kinetic energy production term  $P_k$ ; a modified form of Eq. (9) can be written as:

$$\frac{\partial(\rho u_i k)}{\partial x_i} = \gamma P_k - \beta_1 \rho k \omega + \frac{\partial \left( \left( \mu + \frac{\mu_t}{\sigma_k} \right) \frac{\partial k}{\partial x_i} \right)}{\partial x_i}, \quad (18)$$

As mentioned,  $\gamma$  is calculated by coupling Eqs. (11) & (12). The solution of Eq. (18) & (10) gives the values of  $k$  and  $\omega$  which can be then utilized to obtain the turbulent viscosity  $\mu_t$ :

$$\mu_t = \frac{a \rho k}{\max(a \omega, S F_2)} \quad (19)$$

where  $a$  is a constant and  $F_2$  is another blending function that limits the value of turbulent viscosity inside the boundary layer.

The model of Menter et al. (2006) represents a great breakthrough in transition prediction because it was formulated taking into account only local variables which makes it compatible with modern CFD codes that are 3D and parallel. However, it is worth mentioning that all the model constants recalled in the Menter's model were based on a series of experimental results obtained for external flows. Hence in its original form, this SST transitional turbulence model is not suitable for modelling internal flows, although it has been applied to study the transient turbulent channel flow by Gorji et al. (2014). Model constants proposed originally in the Menter's  $\gamma - Re_{\theta}$  SST transitional turbulence model, in order of appearance in eqs. (13) - (17), are:

$$c_{a1} = 0.5; \quad c_{e1} = 1.0; \quad c_{a2} = 0.03; \quad c_{e2} = 50; \quad \sigma_f = 1.0; \\ c_{\theta t} = 0.03; \quad \sigma_{\theta t} = 10;$$

250

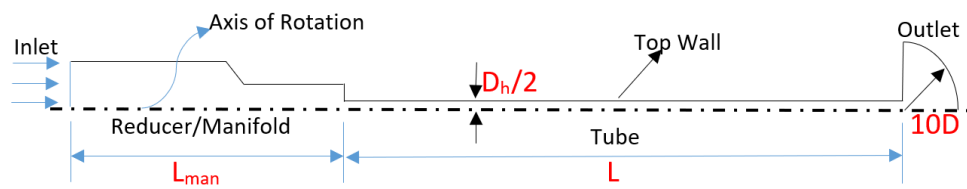
To extend the use of Menter’s model to internal flows, [Abraham et al. \(2008\)](#) later modified the constants of the Eqs. [\(16\)](#) & [\(17\)](#) using an iterative method such that transition in pipe flows was in between a generally accepted range of  $2300 < Re < 4000$ . Coefficients which predicted the transition at a  $Re$  lower than 2300 were not considered. The intermittency coefficient  $c_{e2}$  was increased from 50.0 to 70.0, and  $c_{\theta t}$  was decreased from 0.03 to 0.015. Authors showed that by simply changing two values of the original coefficients of the original Menter’s transitional model ([Menter et al. \(2006\)](#)), transitional characteristics of pipe flows can be predicted. In the current work, similar values of these coefficients as proposed by [Abraham et al. \(2008\)](#), [Minkowycz et al. \(2009\)](#) have been used.

#### 4. Numerical Implementation

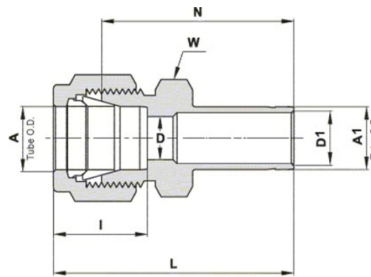
For the implementation of the above explained mathematical model using  $\gamma$ - $Re_{\theta}$  transitional turbulence model, numerical replicas of the experimental channels ([Table 1](#)) were generated in ANSYS-CFX environment ([ANSYS \(2018\)](#)). Computational models of both cross sectional geometries and their respective meshing strategies are detailed in the following:

##### 4.1. Microtube

Test section schematic representing a MT is shown in [Figure 2](#). A commercial reducer is also modelled in the computational domain that connects the gas piping to the MT inlet. Due to axisymmetric nature of the gas flow in MT, only a slice ( $\theta = 10^\circ$ ) is modelled as the computational domain with rotational periodicity boundary condition on the side walls. This allows to save considerable computational time by using a smaller number of mesh elements. Dimensions of the reducer are also shown in [Figure 2b](#). Length ( $L$ ) of the MT varies in different set of numerical simulation and experimental runs. However, dimensions of the reducer and hydraulic diameter ( $D_h$ ) are the same for all cases. MT geometric model is designed in Workbench Design Modeler and is meshed



(a)



Label	Dimension (mm)	Label	Dimension (mm)
A	1.58	I	0.34
A1	6.35	N	27.68
D	1.27	L	31.5

(b)

Figure 2: Computational domain for MT cross section (a), reducer and associated dimensions (b).

using ANSYS meshing software. A structured mesh is generated for the MT as  
 280 shown in Figure 3. Number of divisions along the radial direction ( $r$ ) for the  
 inlet reducer/manifold and outlet are set equal to radial divisions of the MT  
 whereas 15 meshing nodes are used along the length of reducer and outlet.

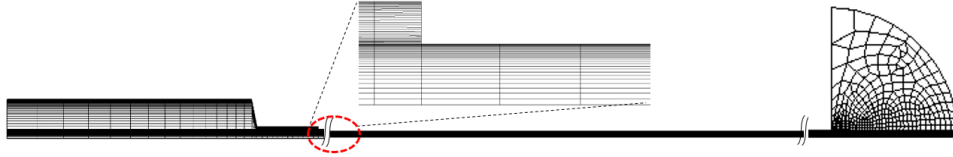


Figure 3: Mesh of the MT geometry.

#### 4.2. Microchannel

To have a better understanding of the flow physics, symmetry boundary  
 285 condition is not applied in the case of rectangular cross-section and therefore  
 a complete 3D geometry as shown in Figure 4 is used as computational domain.  
 The number of node points in the height direction of the MC is reduced  
 accordingly if the height is reduced in the simulation model to maintain better  
 element quality. A structured mesh locally refined at the walls of the MC and  
 290 manifolds is employed. Orthogonality of mesh elements inside MC is between  
 0.95–1 in all the simulated cases. Reducers and manifolds are also simulated  
 along with the MCs. Height of the reducer ( $H_{in}$ , see Figure 4) is 30 mm with  
 an internal diameter of 4 mm. Whereas the diameter of the circular manifolds  
 is 9 mm and height ( $H_{man}$ ) is kept the same as the height of the simulated  
 295 MC ( $H_{man} = h$ ). Dimensions of these parts are chosen based upon the exper-  
 imentally tested MC assembly. The outlet is perfectly symmetric to the inlet  
 manifold and therefore two 90 degrees bends are present in the flow domain and  
 may influence the total pressure drop and hence friction factor evaluation.

#### 4.3. Solution Procedure

300 In order to obtain the desired  $Re$ , mass flow calculated using Eq. (3) is  
 imposed at the inlet of MT/MC. Ideal nitrogen gas enters the reducer/manifold

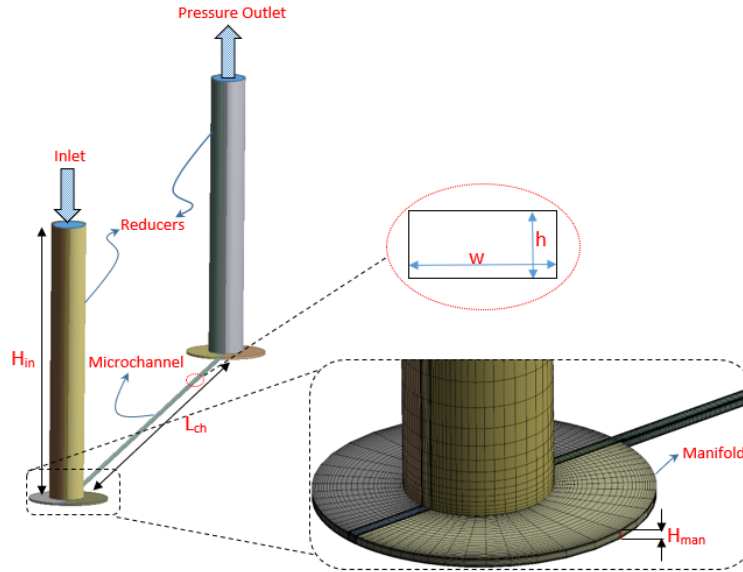


Figure 4: Geometry of the computational domain

for both considered geometries and is vented to the atmosphere using a orthogonal outlet reducer in case of MC and outlet extended domain in MT geometry. The value of turbulence intensity (TI) at the inlet is 5% for all considered  $Re$ , the same value adopted by Abraham et al. (2008). However, in current work  
 305 the inlet boundary condition is set at the entrance of the domain (inlet manifold/reducer) and not at the MC/MT inlet as it was the case with Abraham et al. (2008) and Minkowycz et al. (2009). Hence in laminar regime, due to the fact that reducer section is much longer than manifold, turbulence intensity gets  
 310 dissipated in the first part of the manifold to a smaller value i.e. close to 1%.

Steady state RANS simulations are performed using the SST  $k-\omega$  transitional turbulence model. A modified formulation of  $\gamma-Re_\theta$  transition turbulence model for internal flows is applied based on the coefficients outlined earlier in Sec. 3. High-resolution turbulence numerics are employed with a higher order advection  
 315 scheme available in ANSYS-CFX (ANSYS (2018)). Pseudo time marching is done using a redphysical time step of 0.01s. A convergence criteria of  $10^{-6}$  for RMS residuals of governing equations is chosen while monitor points for pressure

and velocity at the MC/MT inlet and outlet are also observed during successive iterations. In case where residuals stayed higher than convergence criteria, the solution is deemed converged if monitor points did not show any variation for 200 consecutive iterations. Reference pressure of 101 kPa was used for the simulation and all the other pressures are defined with respect to this reference pressure. Due to small measured surface roughness, walls of the MT/MC are treated as smooth in numerical model. A no slip boundary condition is applied at the walls. Energy equation was activated using the total energy option available in CFX. Kinematic viscosity dependence on the gas temperature is defined using Sutherland's law.

$$\mu = \mu_{ref} \left( \frac{T}{T_{ref}} \right)^{\frac{3}{2}} \left( \frac{T_{ref} + S}{T + S} \right), \quad (20)$$

where constants for Nitrogen gas are:

$$\mu_{ref} = 1.7812 \times 10^{-5} \text{ Pa s}$$

$$T_{ref} = 298.15 \text{ K}$$

$$S = 111 \text{ K}$$

Further details of boundary conditions can be seen in Table 4. To estimate

Table 4: Boundary Conditions.

Boundary	Value
Inlet	- mass flow rate: experimental or from Eq. 3) - Turbulence Intensity, TI = 5% - Temperature $T_{in} = 23 \text{ }^\circ\text{C}$
Walls	- No slip - Adiabatic
Outlet	Pressure outlet, $p_{out} = p_{atm}$

the average friction factor, two planes defined at  $x/L$  of 0.0005 and 0.9995 are treated as the inlet and outlet of MC respectively. Analysis results from these planes are further post-processed in MATLAB to evaluate the numerical friction factors using Eq. 1.

#### 4.4. Grid Independence

Three different meshes were utilized for each cross-section where number of elements are systematically increased as shown in Table 5. The difference between the evaluated friction factor was found to be  $\geq 10\%$  from Mesh-A to Mesh-B while it was less than 2% between Mesh-B and Mesh-C. Thus, number of divisions for both cross-sections as shown for Mesh-B in Table 5 are finally utilized. The mesh expansion factor was kept as 1.1 and the first node point was placed such that  $y+$ , which is the non-dimensional distance between the wall and first node point, was  $\leq 1$  in the transitional regime and less than 5 for the highest  $Re$  simulated. Solution accuracy of Mesh-B for both cross sectional geometries

Table 5: Different meshes used for grid independence study.

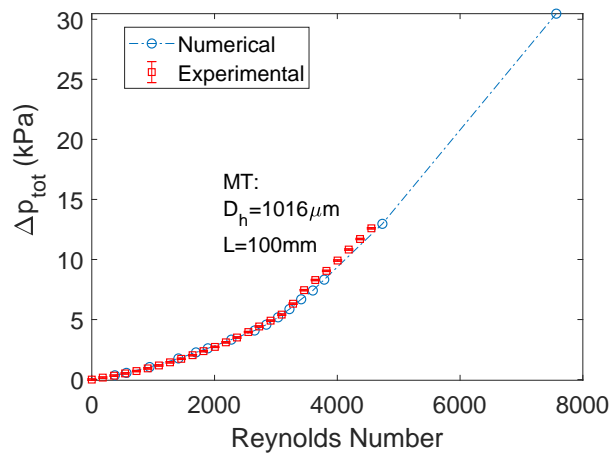
Geometry	A	B	C
MT ( $r \times L \times \theta$ )	$20 \times 100 \times 2$	$40 \times 200 \times 5$	$40 \times 300 \times 10$
MC ( $w \times h \times L$ )	$30 \times 20 \times 100$	$45 \times 30 \times 200$	$50 \times 40 \times 300$

is demonstrated in Figure 5. An excellent agreement between measured and numerical total pressure drop clearly shows that selected mesh and boundary conditions represent the physics of the problem with sufficient accuracy.

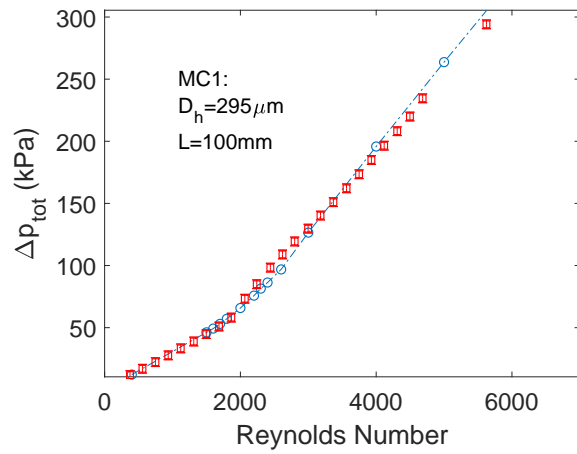
## 5. Results and Discussion

### 5.1. Validation

Laminar to turbulent flow transition is established using the average friction factor curve.  $Re_c$  is defined as the Reynolds number in correspondence of which the friction factor attains its first minimum and then starts to increase. This point is individuated during MATLAB post processing of experimental and numerical results. Theoretical values of friction factor in the laminar regime for considered test sections can be obtained by the Poiseuille equation for circular tubes and the Shah & London correlation (Shah and London (1978), Sahar et al.



(a)



(b)

Figure 5: Comparison of total pressure drop in the assembly for MT (a), and MC1 (b).

(2017) for rectangular channels:

$$f_{c,lam} = \frac{64}{Re} \quad (21)$$

360

$$f_{R,lam} = \frac{96}{Re} (1 - 1.3553\alpha + 1.9467\alpha^2 - 1.7012\alpha^3 + 0.9564\alpha^4 - 0.2537\alpha^5) \quad (22)$$

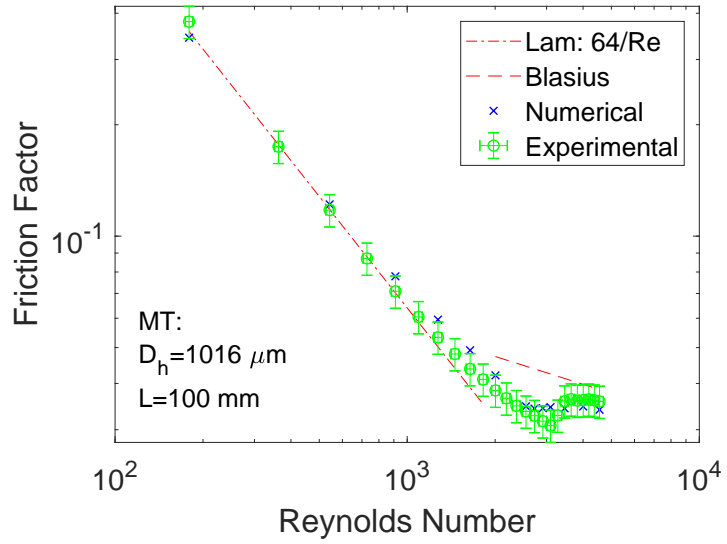
For turbulent regime, Blasius law (smooth tubes) can be used to compare the frictional factor results from experimental and numerical analysis of both cross sections:

$$f_B = 0.3164Re^{-0.25} \quad (23)$$

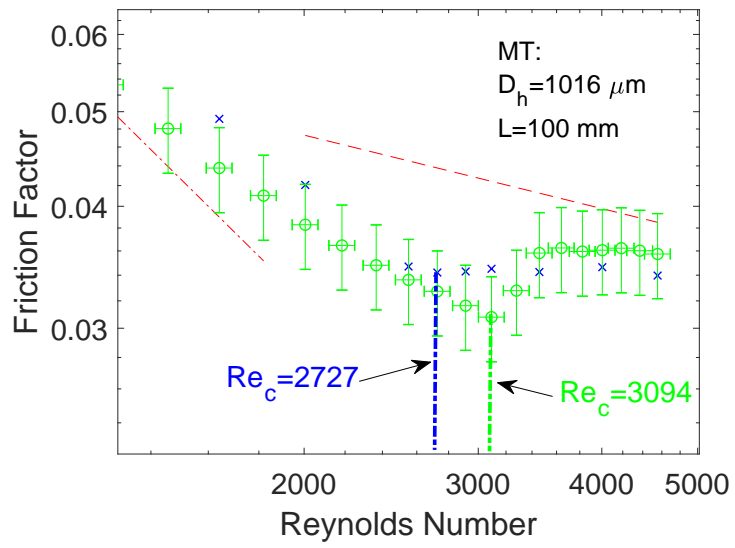
A comparison between numerical and experimental friction factors for circular cross section is made in Figure 6. Numerical results are within the experimental uncertainty in both the laminar and turbulent flow regimes. It can be seen in Figure 6b that the match is excellent in the transitional regime where  $Re_c$  is  $3100 \pm 93$  from experimental results and  $\sim 2727$  using  $\gamma - Re_\theta$  transitional model (-12%). Numerical results in laminar regime are slightly higher than theoretical Poiseuille's law ( $f_{c,lam}$ ) whereas both experimental values and numerical prediction in the turbulent regime are lower than the Blasius law.

A similar comparison between experimental and numerical findings for MC1 is performed in Figure 7. There exists an excellent agreement between the numerical and experimental results in the laminar flow regime where  $f_f$  follows the Shah & London correlation ( $f_{R,lam}$ ). In the turbulent flow regime, both experimental and numerical results are slightly above the Blasius law. However, even in the turbulent regime numerical  $f_f$  is within the uncertainty of experimental results. It is evident from Figure 7b that the model is able to predict the subtle change in slope of  $f_f$  due to the transition from laminar to turbulent flow regime. In fact, the trend of numerical simulation is similar to what is observed in experiments. In transition regime the values of  $f_f$  smoothly connect the limiting cases of laminar and turbulent flow regimes. Contrary to what occurs in external flow where there is a sharp transition to turbulence once disturbances break laminar flow stability, in internal flows a region of fully developed intermittent

375  
380

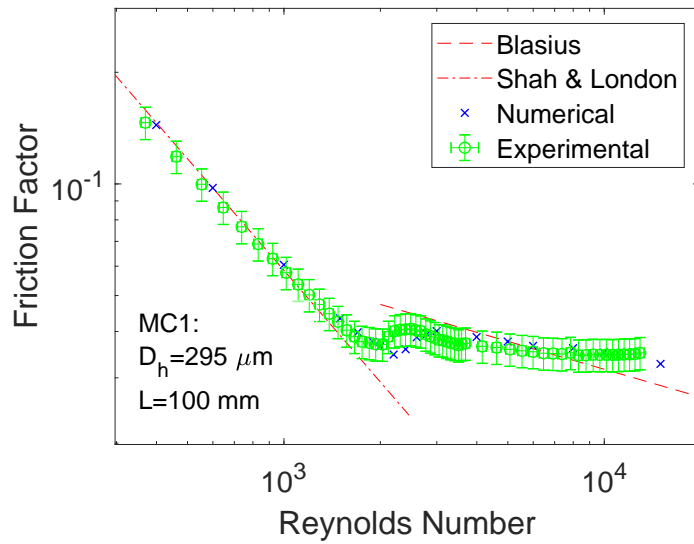


(a)

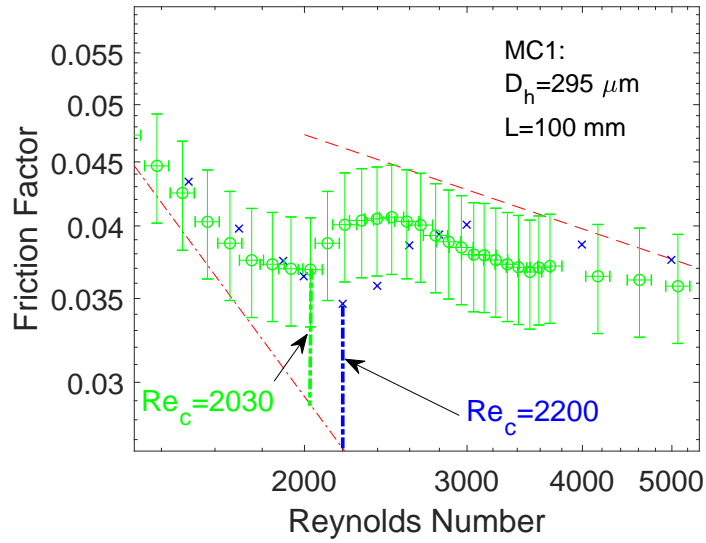


(b)

Figure 6: Friction factor for MT (a), and zoomed laminar-to-turbulent transition region (b).



(a)



(b)

Figure 7: Friction factor for MC1 (a), and zoomed laminar-to-turbulent transition region (b).

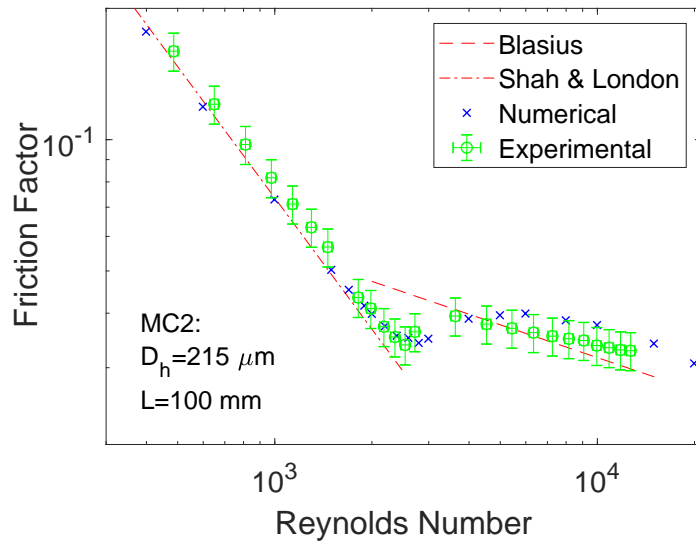
385 flow exists (Abraham et al. (2008, 2010)). This interval could be identified in  
 Figure 7a between  $Re = 1800$  and  $Re = 3000$  for MC1. In this range the  
 agreement between numerical and experimental values is not as good as in the  
 other regimes, but the relative error between the two values remains under 15%.  
 As noted for MT, the intriguing aspect of the  $\gamma - Re_\theta$  transition turbulence mo-  
 390 del is the ability to predict  $Re_c$  with sufficient accuracy. In fact, the difference  
 between experimental and numerical  $Re_c$  is limited also for MC1. Experiments  
 highlighted a  $Re_c$  equal to  $2030 \pm 61$ , whereas numerical one is  $\sim 2200$  (+8%).  
 The correct trend is confirmed by MC2 for which  $f_f$  is reported in Figure 8. In  
 this case experimental  $Re_c$  is observed at  $2536 \pm 76$  whereas model predicts it  
 395 to be  $\sim 2800$  (+10%). An overview of the main results in terms of comparison  
 between experimental and numerical  $Re_c$  is shown in Table 6. Using Menter's  
 $\gamma - Re_\theta$  model as modified by Abraham et al. (2008), the maximum deviation  
 between experimental and numerical values of  $Re_c$  is less than 12 % for all the  
 investigated channels. Moreover,  $Re_c$  showed a decrease from  $\sim 2792$  to  $\sim 2200$   
 400 by increasing the aspect ratio of the rectangular MC ( $\alpha$ ) from 0.24 to 0.7. This  
 decrease is in agreement with the theoretical trend predicted by Obot-Jones  
 Model (Obot (1988)) developed for macro ducts.

Table 6:  $Re_c$  for investigated MT & MCs.

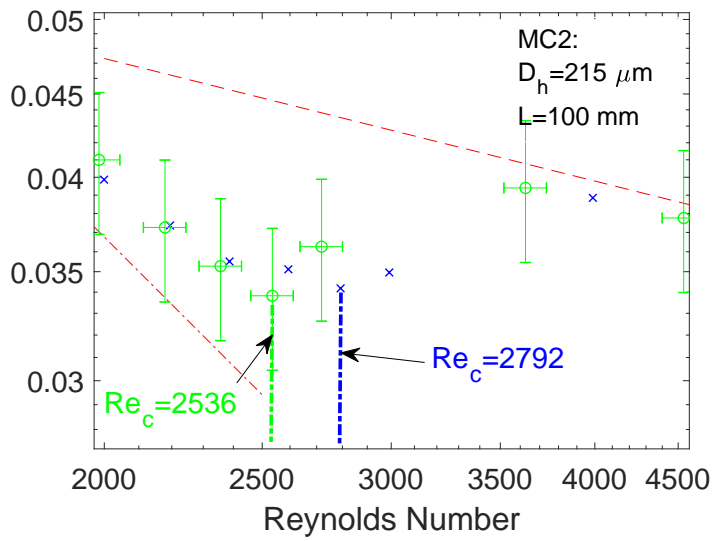
Channel	$D_h$ ( $\mu\text{m}$ )	$\alpha$	Exp. $Re_c$	Num. $Re_c$	Deviation (%)
MT	1016	1	$3094 \pm 93$	$\sim 2727$	11.8
MC1	295	0.7	$2030 \pm 61$	$\sim 2200$	8.4
MC2	213	0.24	$2536 \pm 76$	$\sim 2792$	10

## 5.2. Semi-local friction factor

Laminar-to-turbulent flow transition has been studied in the previous section  
 405 using total pressure loss and therefore average friction factors along the complete  
 length of the MT and MCs were reported. On the other hand, using the Menter's  
 $\gamma - Re_\theta$  turbulence model, the local frictional behavior of the gas flow during



(a)

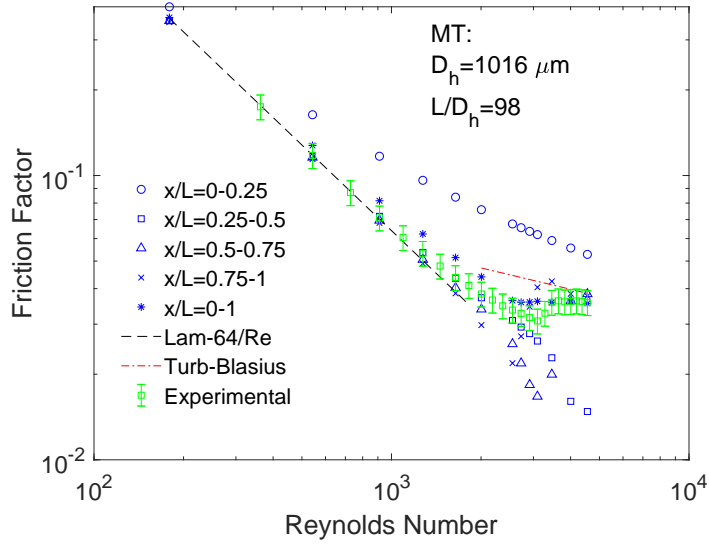


(b)

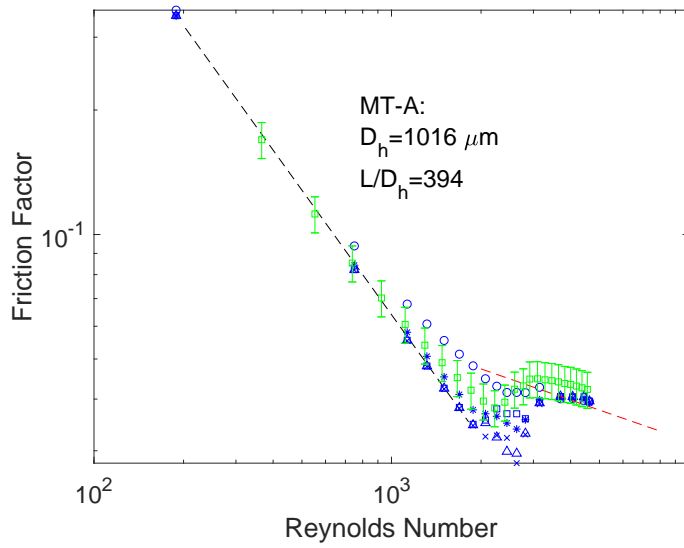
Figure 8: Friction factor for MC2 (a), and zoomed laminar-to-turbulent transition region (b).

the transitional flow regime can be elucidated. In the case of MT, a lower  $f_f$  has been observed (see Figure 6) in the early turbulent regime when compared to the conventional Blasius law. For microchannels, deviation of the turbulent friction factor (higher or lower than) from Blasius law has also been reported by Morini et al. (2007), Kawashima et al. (2016), Yang et al. (2012), Celata et al. (2009). Since the average value of  $f_f$  in microchannels exhibits some deviation from the conventional laws in the turbulent regime, a semi-local analysis of the friction factor values has been performed numerically, by calculating the average value of the friction factor between two fixed axial cross-sections along the channel. Five axial positions along MT have been considered for the semi-local evaluation of the friction factor ( $x = 0L, 0.25L, 0.5L, 0.75L$  and  $L$ ). Semi-local values of  $f_f$  between two consecutive sections are evaluated by employing Eq. 1. An additional numerical run for a MT with the same  $D_h$  (1016  $\mu\text{m}$ ) but an increased length of 400 mm (hereafter referred to as MT-A), is also performed to see any possible effect of the ratio  $L/D_h$  on the laminar-to-turbulent transition as well as local turbulent characteristics of the friction factor (determined numerically).

The comparison between the semi-local values and experimental average friction factor values for the two MTs is shown in Figure 9. As expected, semi-local  $f_f$  is highest in the upstream part of the MT due to strong inlet effects for both MTs. Strictly speaking, the velocity profile for gas flow inside MT, due to the acceleration caused by the gas compressibility, never reaches a developed profile even if the Mach number in these simulations is always lower than 0.2. Therefore, it is not possible to define hydraulic entry length as in the case of incompressible flows. However, propagating the same idea it is evident that for the MT with smaller  $L/D_h$  the developing pressure loss is quite significant and hence causes a higher  $f_f$  when  $x/L$  is between 0-0.25. The experimental as well as the numerical results of  $f_f$  follow the Blasius law in the turbulent flow regime for MT-A (Figure 9b) whereas MT with smaller  $L/D_h$  stays 7% lower than the Blasius law at the highest  $Re$  simulated (Figure 9a). It is interesting to notice that close to the transitional  $Re$ , the semi-local  $f_f$  stays consistently lower than the average theoretical values when  $x/L$  is between 0.25-0.5 as well



(a)



(b)

Figure 9: Semi-local  $f_f$  for MT (a), and MT-A (b).

as 0.5-0.75 whereas it follows the macro laws in the last part of the MT (i.e.
   
 440  $x/L$  between 0.75-1). Therefore, even though in the entrance region, the semi-
   
 local  $f_f$  is quite high, due to its significant decrease in the transitional regime,
   
 the overall average of the evaluated  $f_f$  stays slightly lower than the Blasius
   
 law. Such lower values of the turbulent frictional factor are also evident in the
   
 experimental data of the MT (Figure 9a). On the contrary, such behavior is
   
 445 not observed for the longer tube MT-A and it may be pertinent to MTs having
   
 values of  $L/D_h \leq 100$ . Lower values of the local  $f_f$  compared to fully developed
   
 values are also reported by Abraham et al. (2008) where through the modified
   
 Menter's model described before, authors show that an intermittent nature of
   
 the flow (neither fully laminar nor fully turbulent) may persist inside the tube
   
 450 which results in a lower value of local  $f_f$  compared to the fully developed value
   
 (given by Poiseuille's law) between  $20 < x/D_h < 115$ . Therefore if the length
   
 of the tube is considerably short and hydraulic diameter is big enough (100
   
 mm and  $1016 \mu\text{m}$  in the current case, respectively), local  $f_f$  may stay lower for
   
 most of the length of the MT after an initial hike due to the entrance effects.
   
 455 This ultimately causes the average  $f_f$  to be lower than the Blasius prediction
   
 in the turbulent regime. However, if  $L/D_h$  is reduced further beyond a point,
   
 the whole length of the MT is strongly influenced by the entrance effects and
   
 the apparent  $f_f$  is higher than the conventional laws. This is evident from
   
 all the presented results in the range  $x/L = 0-0.25$  where the semi-local  $f_f$  is
   
 460 much higher than the other semi-local values of the friction factor far from the
   
 entrance. Similar findings were reported by Cheng et al. (2017) where they
   
 recommended using  $L/D_h > 100$  for the evaluation of  $f_f$  without significant
   
 differences from the conventional theory. Barlak et al. (2011) also found that
   
 MTs having a  $L/D_h$  smaller than 100, seriously affect the overall  $f_f$  due to the
   
 465 entrance effects, by determining higher values of  $f_f$  than the Blasius prediction
   
 in the turbulent regime. On the other hand, for the tube with  $L/D_h > 100$ 
  
 (MT-A), the semi-local  $f_f$  far from the entrance region ( $x/L = 0.5 - 0.75$  and
   
 $x/L = 0.75 - 1$ ) follows the conventional laws in the laminar as well as the
   
 turbulent regimes by confirming the complete agreement with the conventional

470 theory even for the microchannels. The semi-local values of the  $f_f$  shown in  
 Figure 9 demonstrate that the higher values of the  $f_f$  close to the entrance  
 region of the channel are the main motivation for the deviation of the average  
 overall friction factor from the Poiseuille's law in the laminar regime when  $Re$   
 increases. On the contrary, the overall friction factor is only marginally higher  
 475 than the Blasius correlation in the turbulent regime. From the experimental  
 results shown in Figure 9, it can be deduced how MT with  $L/D_h \leq 100$  shows  
 a delayed transition compared to the longer MT-A.  $Re_c$  decreased from 3094  
 in the case of  $L/D_h = 98$  to 2223 for  $L/D_h = 398$ . On the contrary, numerical  
 results show that  $Re_c$  decreased slightly from  $\sim 2727$  to  $\sim 2635$  by increasing  
 480 the  $L/D_h$  from 98 to 398. On this point, the comparison between numerical  
 and experimental results is inconclusive and more data needs to be collected to  
 better understand the effect of  $L/D_h$  ratio on the critical Reynolds number.

## 6. Conclusions

In this paper, it has been demonstrated that the laminar-to-turbulent tran-  
 485 sition for gas microflows can be estimated with acceptable accuracy using Men-  
 ter's  $\gamma - Re_\theta$  transitional turbulence model (Menter et al. (2006)) as modified  
 by Abraham et al. (2008). Validation of the model with experimental results  
 showed that the modified Menter's model predicted the critical Reynolds num-  
 ber linked to the laminar-to-turbulent transition ( $Re_c$ ) with a maximum er-  
 490 ror of 11.8% for all the tested channels having different cross-sections and  $D_h$   
 values. Local frictional characteristics showed that for the short MT having  
 $L/D_h \leq 100$ , the semi-local  $f_f$  are significantly lower than the conventional va-  
 lues for a large part of the MT length, during the transitional and early turbulent  
 regimes. This causes the overall  $f_f$  to be lower than the Blasius correlation in  
 495 the turbulent regime whereas for channels having  $L/D_h > 100$ , no deviation  
 from the Blasius law is observed.

## Credit Author Statement

Danish Rehman: Formal analysis, Investigation, Methodology, Validation, Writing—original draft; Gian Luca Morini: Funding acquisition, Methodology, Supervision, Writing—review & editing

## Acknowledgements

This research received funding from the European Union’s Framework Programme for Research and Innovation Horizon 2020 (2014–2020) under the Marie Skłodowska-Curie Grant Agreement No. 643095 (MIGRATE Project).

## Nomenclature

$A$	Cross section area of the microchannel/microtube
$c_{\gamma,2}$	Transitional model constant
$c_{\theta,t}$	Transitional model constant
$D_h$	Hydraulic diameter
$E_1, E_2$	Intermittency destruction terms
$F_1, F_2$	Blending functions in SST-k- $\omega$ turbulence model
$f_f$	Fanning friction factor
$f_{c,lam}$	Laminar friction factor for circular cross section
$f_{R,lam}$	Laminar friction factor for rectangular cross section
$f_B$	Blasius friction factor
$\dot{G}$	Mass flux
$h$	Height of the microchannel
$H_{man}$	Height of the manifold
$H_{in}$	Height of the reducer
$k$	Turbulent kinetic energy
$\dot{m}$	Mass flow rate
$p$	Pressure
$P_k$	Rate of kinetic energy production

$P_{\gamma,1}, P_{\gamma,2}$	Intermittency production terms
$P_{\theta,t}$	Production term for the transition onset Reynolds number
$R$	Specific gas constant
$Re$	Reynolds Number
$Re_{\theta,t}$	Transition momentum thickness Reynolds number
$S$	Absolute value of the shear strain
$T$	Temperature
$u$	Velocity of the fluid
$w$	Width of the microchannel
$L$	Length of the the microchannel/microtube
$y+$	Non-dimensional distance between the wall and first node element

*Greek Symbols*

$\alpha$	Aspect ratio of the microchannel
$\beta_1, \beta_2$	SST model constants
$\gamma$	Intermittency factor
$\epsilon$	Surface roughness of the microchannel/microtube
$\mu$	Dynamic viscosity of the fluid
$\mu_t$	Turbulent/eddy viscosity
$\nu$	Kinematic viscosity of the fluid
$\rho$	Density
$\tau$	Shear stress
$\chi$	SST model constant
$\omega$	Specific rate of turbulent destruction
$\Omega$	Magnitude of the absolute vorticity rate

### *Subscripts*

<i>av</i>	Averaged over the whole length of the microtube/microchannel
<i>c</i>	Critical
<i>i</i>	Cartesian components of the flow quantity
<i>in</i>	at the inlet of the microtube/microchannel
<i>out</i>	at the outlet of the microtube/microchannel
<i>tot</i>	Total (static and dynamic) part of the flow quantity
<i>w</i>	Wall
<i>x</i>	Flow quantity at cross section located at distance 'x' from the inlet

### *Abbreviations*

	2D/3D	Two dimensional and three dimensional
	CFD	Computational fluid dynamics
	DNS	Direct numerical simulation
	LES	Large eddy simulation
	MT	Microtube
510	MC	Microchannel
	PMMA	Poly methyl methacrylate (acrylic)
	RANS	Reynolds-averaged Navier–Stokes equations
	RMS	Root mean squared
	SST	Shear Stress Transport
	S&L	Shah and London

### **References**

Abraham J, Sparrow E, Tong J. Breakdown of laminar pipe flow into transitional intermittency and subsequent attainment of fully developed intermittent or turbulent flow. *Numerical Heat Transfer, Part B: Fundamentals* 2008;54(2):103–15.

Abraham J, Sparrow E, Tong J, Bettenhausen D. Internal flows which transit from turbulent through intermittent to laminar. *International Journal of*

- Thermal Sciences 2010;49(2):256–63. doi:[10.1016/j.ijthermalsci.2009.07.013](https://doi.org/10.1016/j.ijthermalsci.2009.07.013).
- 520 Adams TM, Dowling MF, Abdelkhalik S, Jeter SM. Applicability of traditional turbulent single-phase forced convection correlations to non-circular microchannels. *Int J Heat and Mass Transfer* 1999;42(23):4411–5.
- ANSYS . Cfx version 18.1 manual. ANSYS, Inc, Cannosburg, PA 2018;.
- Asadi M, Xie G, Sunden B. A review of heat transfer and pressure drop characteristics of single and two-phase microchannels. *Int J Heat and Mass Transfer* 525 2014;79:34–53.
- Avila K, Moxey D, de Lozar A, Avila M, Barkley D, Hof B. The onset of turbulence in pipe flow. *Science* 2011;333(6039). doi:[10.1126/science.1203223](https://doi.org/10.1126/science.1203223).
- Barkley D, Song B, Mukund V, Lemoult G, Avila M, Hof B. Eliminating 530 turbulence in spatially intermittent flows. *Science* 2010;327(5972):1491–4. doi:[10.1126/science.1186091](https://doi.org/10.1126/science.1186091).
- Barkley D, Song B, Mukund V, Lemoult G, Avila M, Hof B. The rise of fully turbulent flow. *Nature* 2011;526:550–3. doi:[10.1126/science.1203223](https://doi.org/10.1126/science.1203223).
- Barlak S, Yapıcı S, Sara O. Experimental investigation of pressure drop and friction factor for water flow in microtubes. *International Journal of Thermal Sciences* 2011;50(3):361 –8. URL: <http://www.sciencedirect.com/science/article/pii/S1290072910002577>. doi:<https://doi.org/10.1016/j.ijthermalsci.2010.08.018>; nano, Micro and Mini Channels.
- 540 Celata G, Lorenzini M, Morini G. Friction factor in micropipe gas flow under laminar, transition and turbulent flow regime. *Int J Heat Fluid Flow* 2009;30:814–22.
- Cheng J, Li H, Zhu Z, Tao Z. Numerical simulation of flow transition in a rectangular microchannel. In: ICHMT DIGITAL LIBRARY ONLINE. Begel 545 House Inc.; 2017. p. 1419–28.

- Choi S, Barron R, Warrington R. Fluid flow and heat transfer in microtubes. *Micromechanical Sensors, Actuators, and Systems*, ASME 1991;:123–34.
- Dixit T, Ghosh I. Review of micro- and mini-channel heat sinks and heat exchangers for single phase fluids. *Renewable and Sustainable Energy Reviews* 2015;41:1298–311. 550
- Gorji S, Seddighi M, Ariyaratne C, Vardy A, O’Donoghue T, Pokrajac D, He S. A comparative study of turbulence models in a transient channel flow. *Computers Fluids* 2014;89:111–23. URL: <http://www.sciencedirect.com/science/article/pii/S0045793013004209>. 555 doi:<https://doi.org/10.1016/j.compfluid.2013.10.037>.
- Harms TM, Kazmierczak MJ, Gerner FM. Developing convective heat transfer in deep rectangular microchannels. *Int J Heat and Fluid Flow* 1999;20(2):149–57.
- Hong C, Nakamura T, Asako Y, Ueno I. Semi-local friction factor of turbulent gas flow through rectangular microchannels. *International Journal of Heat and Mass Transfer* 2016;98:643–9. 560
- Kandlikar SG, Schmitt D, Carrano AL, Taylor JB. Characterization of surface roughness effects on pressure drop in single-phase flow in minichannels. *Physics of Fluids* 2005;17(100606). doi:<https://doi.org/10.1063/1.1896985>.
- Kawashima D, Asako T. Data reduction of friction factor for compressible flow in micro-channels. *International Journal of Heat and Mass Transfer* 2014;77:257–61. 565
- Kawashima D, Yamada T, Hong C, Asako Y. Mach number at outlet plane of a straight micro-tube. *Proceedings of the Institution of Mechanical Engineers, Part C: Journal of Mechanical Engineering Science* 2016;230(19):3420–30. URL: <https://doi.org/10.1177/0954406215614598>, doi:[10.1177/0954406215614598](https://doi.org/10.1177/0954406215614598). arXiv:<https://doi.org/10.1177/0954406215614598>. 570

- Kühnen J, Song B, Scarselli D, Budanur NB, Riedl M, Willis AP, Hof MAB.  
Destabilizing turbulence in pipe flow. *Nature Physics* 2018;14.
- 575 Kim B. An experimental study on fully developed laminar flow and heat transfer  
in rectangular microchannels. *International Journal of Heat and Fluid Flow*  
2016;62:224–32.
- Launder B, Spalding D. The numerical computation of turbulent flows.  
*Computer Methods in Applied Mechanics and Engineering* 1974;3(2):269  
580 –89. URL: [http://www.sciencedirect.com/science/article/pii/](http://www.sciencedirect.com/science/article/pii/0045782574900292)  
[0045782574900292](http://www.sciencedirect.com/science/article/pii/0045782574900292). doi:[https://doi.org/10.1016/0045-7825\(74\)](https://doi.org/10.1016/0045-7825(74)90029-2)  
[90029-2](https://doi.org/10.1016/0045-7825(74)90029-2).
- Li H, Olsen MG. Aspect ratio effects on turbulent and transitional flow in  
rectangular microchannels as measured with micropiv. *Journal of fluids en-*  
585 *gineering* 2006;128(2):305–15.
- Menter F, Langtry R. Transition modelling for turbomachinery flows. In: *Low  
Reynolds Number Aerodynamics and Transition*. InTech; 2012. .
- Menter FR. Two-equation eddy-viscosity turbulence models for engineering  
applications. *AIAA journal* 1994;32(8):1598–605.
- 590 Menter FR, Langtry RB, Likki S, Suzen Y, Huang P, Völker S. A correlation-  
based transition model using local variables—part i: model formulation. *Jour-*  
*nal of turbomachinery* 2006;128(3):413–22.
- Minkowycz W, Abraham J, Sparrow E. Numerical simulation of laminar break-  
down and subsequent intermittent and turbulent flow in parallel-plate chan-  
595 nels: Effects of inlet velocity profile and turbulence intensity. *International  
Journal of Heat and Mass Transfer* 2009;52(17-18):4040–6.
- Morini G. Laminar to turbulent flow transition in microchannels. *Microscale  
Thermophysical Eng* 2004a;8:15–30.

- Morini G, Lorenzini M, Salvigni S, Spiga M. Analysis of laminar-to-turbulent  
600 transition for isothermal gas flows in microchannels. *Microfluidics and Nanofluidics* 2009;7(2):181–90.
- Morini GL. Single-phase convective heat transfer in microchannels: a review of experimental results. *International journal of thermal sciences* 2004b;43(7):631–51.
- 605 Morini GL, Lorenzini M, Colin S, Geoffroy S. Experimental analysis of pressure drop and laminar to turbulent transition for gas flows in smooth microtubes. *Heat Transfer Engineering* 2007;28(8-9):670–9. doi:[10.1080/01457630701326308](https://doi.org/10.1080/01457630701326308).
- Obot N. Determination of incompressible flow friction in smooth circular and  
610 noncircular passages: A generalized approach including validation of the nearly century old hydraulic diameter concept. *J Fluids Eng* 1988;110:431–40. doi:<https://doi.org/10.1115/1.3243574>.
- Peiyi W, Little W. Measurement of friction factors for the flow of gases in very fine channels used for microminiature joule-thomson refrigerators. *Cryogenics* 1983;23(5):273 –7. URL: <http://www.sciencedirect.com/science/article/pii/0011227583901509>. doi:[https://doi.org/10.1016/0011-2275\(83\)90150-9](https://doi.org/10.1016/0011-2275(83)90150-9).
- 615 Peng X, Peterson G, Wang B. Frictional flow characteristics of water flowing through rectangular microchannels. *Experimental Heat Transfer An International Journal* 1994;7(4):249–64.
- 620 Rehman D, Morini GL, Hong C. A comparison of data reduction methods for average friction factor calculation of adiabatic gas flows in microchannels. *Micromachines* 2019;10(3):171.
- Reynolds O. Xxix. an experimental investigation of the circumstances which  
625 determine whether the motion of water shall be direct or sinuous, and of the

- law of resistance in parallel channels. *Phil Trans R Soc* 1883;174. doi:<https://doi.org/10.1098/rstl.1883.0029>.
- Sahar AM, Wissink J, Mahmoud MM, Karayiannis TG, Ishak MSA. Effect of hydraulic diameter and aspect ratio on single phase flow and heat transfer in a rectangular microchannel. *Applied Thermal Engineering* 2017;115:793–814. 630
- Shah R, London A. *Laminar Flow Forced Convection in Ducts*. Academic Press, 1978. URL: <http://www.sciencedirect.com/science/article/pii/B9780120200511500061>. doi:<https://doi.org/10.1016/B978-0-12-020051-1.50006-1>.
- Tuckerman D, Pease R. High-performance heat sinking for vlsi. *IEEE Electron Device Lett* 1981;5:126–9. doi:[doi:10.1109/EDL.1981.25367](https://doi.org/10.1109/EDL.1981.25367). 635
- Wibel W, Ehrhard P. Experiments on the laminar/turbulent transition of liquid flows in rectangular microchannels. *Heat Transfer Engineering* 2009;30(1-2):1298–311. doi:<https://doi.org/10.1080/01457630802293449>.
- Wilcox DC. Re-assessment of the scale-determining equation for advanced turbulence models. *AIAA journal* 1988;26(11):1299–310. 640
- Wilcox DC. Formulation of the k-w turbulence model revisited. *AIAA journal* 2008;46(11):2823–38.
- Wu X, Moin P, Adrian RJ, , Baltzer JR. Osborne reynolds pipe flow: Direct simulation from laminar through gradual transition to fully developed turbulence. *PNAS* 2015;112(26):7920–4. doi:<https://doi.org/10.1073/pnas.1509451112>. 645
- Yang Y. *Experimental and Numerical Analysis of Gas Forced Convection through Microtubes and Micro Heat Exchangers*. PhD dissertation, Alma Mater Studiorum- Universita di Bologna, 2012. 650
- Yang Y, Brandner J, Morini G. Hydraulic and thermal design of a gas microchannel heat exchanger. *Journal of Physics: Conference Series* 2012;362. doi:[10.1088/1742-6596/362/1/012023](https://doi.org/10.1088/1742-6596/362/1/012023).